Hindawi
Shock and Vibration
Volume 2019, Article ID 2094378, 18 pages
https://doi.org/10.1155/2019/2094378

Research Article

Numerical Investigation into Evolution of Crack and Stress in Residual Coal Pillars under the Influence of Longwall Mining of the Adjacent Underlying Coal Seam

Xin Wang,[1,2] Yuechao Wu,[1] Xuehua Li,[1] and Shun Liang[1,2]

[1]*State Key Laboratory of Coal Resources and Safe Mining, School of Mines, China University of Mining and Technology, Xuzhou 221116, China*
[2]*College of Mining Engineering, Liaoning Technical University, Fuxin, Liaoning 123000, China*

Correspondence should be addressed to Shun Liang; 5756@cumt.edu.cn

Received 30 July 2018; Revised 2 December 2018; Accepted 20 January 2019; Published 17 February 2019

Academic Editor: Adam Glowacz

Longwall mining of the adjacent coal seam with the presence of residual coal pillars overlying the seam can result in abnormal strata pressure and severe overburden failure, which poses a significant threat to mining safety. The threat is mainly manifested in the form of intense coal or rock burst and hazardous interconnection between gobs. This study employed the universal distinct element code (UDEC) to investigate the microscopic failure mechanism of the overlying residual coal pillars under the influence of longwall mining of an adjacent underlying coal seam in Yuanbaowan coal mine, China. Using the Voronoi method, we innovatively visualized the evolution of cracks in residual pillars, revealed the mechanism behind the failure of pillars, and explored the evolution and distribution of abutment stress. Also, strata movement characteristics during underlying panel extraction have been surveyed. Based on the modeling results, effective measures are proposed to ensure safe mining under residual coal pillars. This study might provide a certain reference for safe extraction of multiple seams in Datong Coalfield, China, and also in the central and western Appalachian Basin, United States, where many mining activities are carried out under residual pillars.

1. Introduction

Coal seams in Datong coalfield show distinctive characteristics. Most of them occur close to each other and are gently inclined shallow thick coal seams with fewer faults and hard roof. In the past, small-scale lane mining and room-and-pillar mining methods were employed to extract shallow coal seams [1]. As a result, a significant number of coal pillars are left in gobs. Residual coal pillars along with irregular gobs bring a series of difficulties to longwall mining of underlying adjoining coal seams [2–8]. Effects of multiple seam interactions and pillar instability include roof falls, rib spalling, floor heave, and bumps which can seriously disrupt mining operations and threaten the safety of miners [7–17]. In early 2006, a West Virginia coal miner was killed by a rib roll which occurred in a high-stress zone beneath a remnant structure in an overlying mine [18].

Critical issues standing out in safe extraction of the underlying abutting coal seams under residual pillars are the effective control measures of roofs [4, 5, 7–10]. Many scholars have made a detailed study on the relation between overburden rock structures and support-surrounding rock systems using theoretical analysis, numerical modeling, and in situ experiments [4–8, 10–17, 19–25]. Based on the catastrophe theory, Wang et al. established a cusp catastrophe model for the study of the stability of residual coal pillars left by room mining in shallow seams and explored the catastrophic failure characteristics of coal pillars [3–5]. Using physical simulation and 3DEC numerical modeling, both movement characteristics of the overlying strata of shallow coal seams and the hydraulic support jamming mechanism in longwall mining of seams under residual pillars are investigated. Yang et al. regarded two abutting seams as a composite structure system and proposed a simplified model

to investigate the stress and movement characteristics of the system [6]. With the proposed model, the critical condition for roofs under residual pillars to maintain stability is derived; also, the effects of the location of immediate roof fractures and the dimension of residual pillars on roof stability are investigated. According to the loading characteristics of hydraulic support, Wang divided the strata overlying the fully mechanized coalface of a seam under a gob into four types, analyzed the caving characteristics of the strata of various types, and explored the corresponding bearing characteristics of hydraulic support [19]. Ju et al. examined the failure characteristics of overburden rock structures as the coalface under pillars is progressing [20–23]. They concluded that hydraulic support jamming is mainly attributable to the structural instability of critical rock blocks above residual pillars. Based on this, they proposed some measures against hydraulic support jamming. It can be seen that the above studies have made bold attempts to study issues concerning mining under residual pillars. To be more specific, the issues cover the failure characteristics of residual coal pillars, the stability of roof under residual coal pillars, and the weighting characteristics of roofs [2, 26–32]. However, studies to date have mainly investigated pillar and roof failures from a macro perspective, whereas few efforts have been devoted to the microscopic mechanism behind these failures. A good microunderstanding of the evolution of stress and crack in residual coal pillars and the progressive collapse process during longwall mining of underlying seam is of great importance to make clear the relation among hydraulic supports, roofs, and pillars. Therefore, to achieve safe mining under residual pillars, it is of great necessity to carry out microstudies on the progressive failure of pillars.

This study took the #6 coal seam in the Yuanbaowan Mine, China, as an example and employed the universal distinct element code (UDEC) to investigate the failure mechanism of residual coal pillars under the influence of longwall mining of the underlying adjoining seam. Above the #6 coal seam lays the #4 coal seam where residual pillars are located. Using the Voronoi method [33–41], we discretized meshes for the #4 coal seam and interburden between #4 seam and #6 seam, to better visualize the evolution of cracks. The blocks that can be either rigid or deformable are separated by interfaces which are viewed as contacts. With the custom-developed Fish language, we quantified the number of the tensile and shear cracks. As a result, the progressive failure of residual pillars was satisfactorily modeled. Also, we modeled the effect of residual pillars on the scope of influence and distribution of the front abutment stress in the underlying abutting seam during panel extraction. Based on the modeling results, some measures are also proposed to ensure safe mining under residual coal pillars. This study might have a certain reference value for the safe extraction of coal seams in Datong or Shuozhou Coalfield, China, where many mining activities are implemented under residual pillars.

Affiliated to China National Coal Group Corporation, the Shanxi Huayu Yuanbaowan coal mine is a consolidated mine. Mining starts from the #6 coal seam, with 6104 fully mechanized face as the first coalface. The 6105 fully mechanized face is the successive coalface. Above 6104 and 6105 coalfaces lay in the #4 coal seam where pillars are left in place as a result of small-scale lane mining and room-and-pillar mining (Figure 1). The underground site survey shows that, though apparent cracks are observed on the surface of some coal pillars, the roof of mined rooms in the #4 coal seam and most residual pillars in gobs are still in fairly good condition (Figure 2), demonstrating favorable bearing capacity. Figure 2(a) is a site photo that shows the exposed roof of mined rooms in the #4 coal seam. Figure 2(b) shows the roof caving in one laneway. Subject to long-term loading, weathering, and water intrusion, the residual coal pillars dotted around the gob exhibit varying degrees of erosion and spalling (Figures 2(b)–2(d)).

According to the mining practice of the nearby mines, the #4 seam could pose a significant threat to longwall mining of the #6 coal seam. The threat mainly manifests itself in the form of intense roof weighting and hazardous interconnection between the gobs, as illustrated in Figure 3. Resulting from the extraction of the #6 seam and the failure of the residual coal pillars in the #4 seam, the intense roof weighting could exert dynamic impacts on the coalface in production, leading to rock burst and hydraulic support jamming or damage. The interconnection between the gobs results from the unfavorable caving of the roof above the coalface. Once the mined-out areas are interconnected, hazardous or poisonous gas could enter into the #6 seam coalface, posing a significant threat to personal safety.

2. Mining and Geological Conditions

Yuanbaowan mine is about 4.2 km long in the East-West direction and 2.1 km wide in the North-South direction. The #4 seam and #6 seam belonging to the carboniferous Taiyuan Formation are the two primary minable coal seams in the mine. Mining starts from the #6 seam, above which lays the #4 seam where residual pillars are left in place. The #6 seam is 150–160 m deep, with a thickness of 2.7–5.2 m (on average 3.4 m). The #4 seam is 7.2 m thick on average, overlying the #6 seam with a vertical distance of 8.56–19.72 m (on average 16 m). Between the #6 seam and #4 seam are the coarse sandstone, fine sandstone, and sandy mudstone. Figure 4 shows the stratigraphic column of the borehole YZK2102 in 6105 longwall working face.

The 6104 face is the first coalface in the #6 seam. This coalface is 2.8 high and 180 m long, with an advance length of 1080 m. The longwall fully mechanized top caving method is employed in the coalface to extract the coal resources. The 6105 face is the successive coalface. Figure 5 is the projection plane that depicts the spatial relationship between the gob in the #4 seam (the area delineated by the red dotted line) and the coalfaces in the #6 seam.

3. Model Establishment

3.1. Model Construction. The residual coal pillars left in the #4 seam act as the carriers that connect the seam roof and floor. Therefore, the stability of these coal pillars exerts a

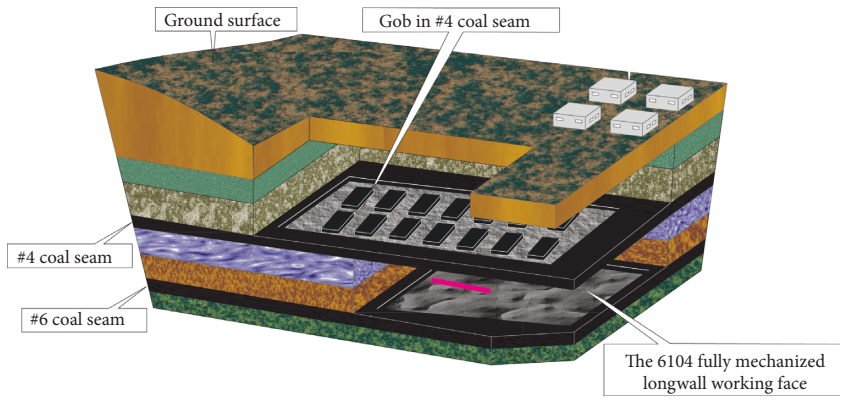

Figure 1: Schematic diagram of mining status in the Yuanbaowan coal mine.

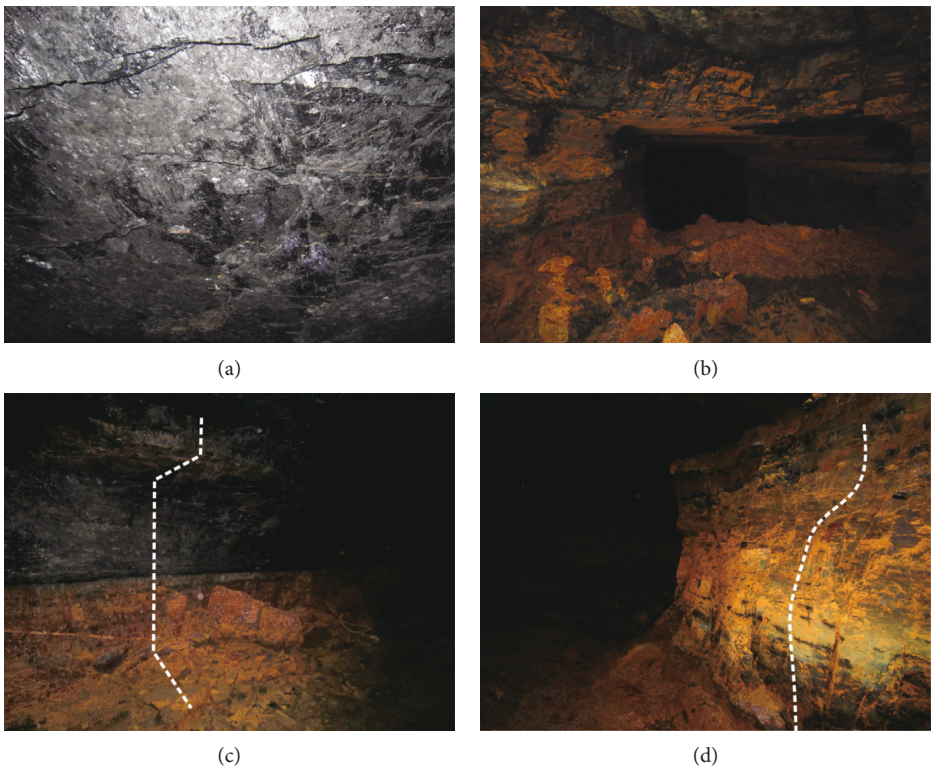

Figure 2: Site photos showing the failure condition of the roof and coal pillars in the #4 seam. (a) Cracks in exposed roof of the #4 seam. (b) Roof caving in one laneway of the #4 seam. (c) Lateral spalling of a coal pillar. (d) Splitting failure of the coal pillar.

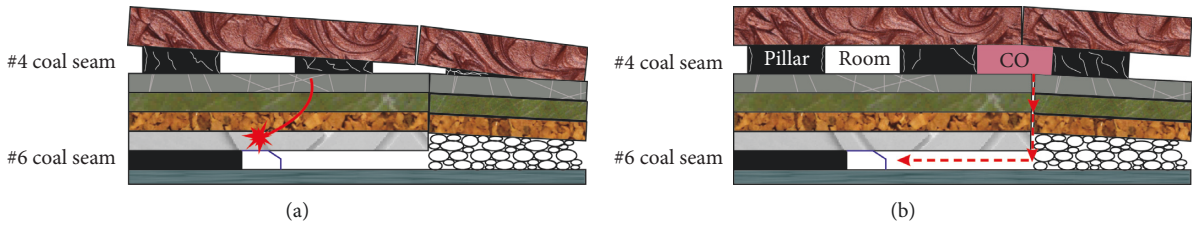

Figure 3: Schematic diagram of potential hazards at the #6 seam coalface in Yuanbaowan mine. (a) Dynamic impacts resulting from sudden fracture of the exposing roof. (b) Entrance of hazardous and poisonous gas into the panel after the interconnection between the gobs.

direct effect on the strata pressure occurring in the underlying #6 seam during panel extraction. The underground site survey shows that the mined-out area is irregular, and the coal pillars vary slightly in shape and dimension (Figure 2). To facilitate model construction, we simplified the geometrical parameters of the residual pillars. In the model,

Number	Lithology	Log	Thickness
1	Siltstone		8.0 m
2	#3-1 coal seam		4.4 m
3	Mudstone		6.6 m
4	#3-2 coal seam		1.4 m
5	Sandy mudstone		4.0 m
6	Fine sandstone		1.6 m
7	Coarse sandstone		5.5 m
8	Fine sandstone		2.0 m
9	Coarse sandstone		1.0 m
10	#4 coal seam		6.1 m
11	Sandy mudstone		5.4 m
12	Fine sandstone		3.7 m
13	Coarse sandstone		7.5 m
14	#6 coal seam		3.4 m
15	Mudstone		4.0 m
16	Sandy mudstone		3.0 m
17	Fine sandstone		5.4 m

Figure 4: Stratigraphic column of borehole YZK2102 in 6105 longwall working face.

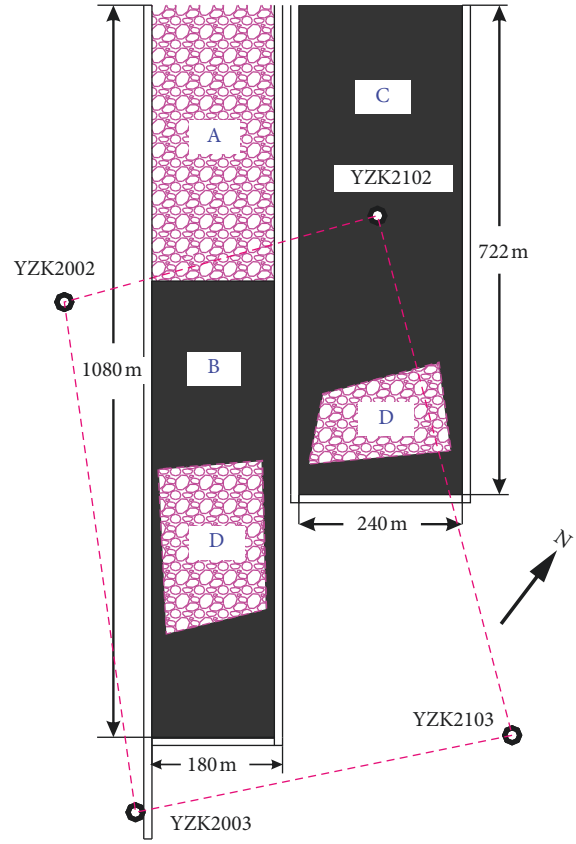

Figure 5: Projection plane depicting the spatial relationship between the gob in the #4 seam and the panels in the #6 seam. A: longwall mining gob in the #4 seam; B: mining area of the 6104 fully mechanized face; C: the 6105 fully mechanized face; D: the room mining gob in the #4 seam.

the coal pillar is 6 m high and 15 m wide. To model the most undesirable situation, we design the width of the room as 30 m in the model, which is the maximum width of the room according to our site survey. Note the longwall panel in the lower seam is excavated along the direction perpendicular to the axis of the pillars in the upper seam. In this case, the residual coal pillars could suffer the maximum loading from the roof strata and exert more severe effects on the floor.

In this study, we choose the universal distinct element code software (UDEC) as it can realistically model the crack initiation and propagation in rocks. In UDEC, the computational domain is discretized into blocks using a finite number of intersecting discontinuities. A physical discontinuity is created when the stress level at the interface between blocks exceeds a threshold value either in tension or shear. Using the polygonal block, rock failure is captured either in the form of plastic yielding of the rock matrix or displacements of the discontinuities due to Voronoi tessellation. The objective of this study is mainly to investigate the evolution of crack and stress within the residual coal pillars and failure mechanism of the pillars during longwall mining of the underlying seam. Meanwhile, considering the efficiency of model convergence, which largely depends on the size and number of blocks, we incorporate two pillars and three rooms in the upper #4 coal seam in the model. Figure 6 shows the configuration of the longwall model using the polygonal command in UDEC. The model is 250 m in length and 120 m in height. In the vertical direction, the model is constructed in strict accordance with the stratigraphic column shown in Figure 4.

As the emphasis of this study is to investigate the microscopic mechanism of failure within the residual coal pillars in the upper seam and within the interburden, we discretize both the pillars and interburden using the Voronoi method [33–41]. Given the sizes of the whole model and the pillars and rooms within the #4 seam, we set the average edge length of the polygons within the pillars as 0.5 m, which is approximately one-tenth of the shortest side length of the pillar's cross section (6 m, the height of the coal pillar). To facilitate the study of the roof failure during the panel advance in #6 seam, we discretize the interburden between seams into polygons as well. The average edge length of these polygons is 1.5 m, which is also about tenth of the thickness of the interburden between the #4 seam and #6 seam (16.6 m). This setting can well represent crack generation

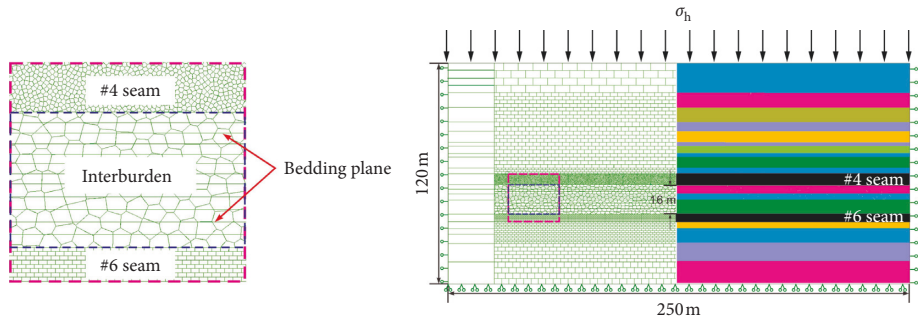

Figure 6: Model geometry and boundary conditions of the model built using the polygonal command in UDEC [33].

and propagation in the coal mass and can reliably reveal the failure mode of the pillar. At the same time, it could not be time consuming. The other strata, including the #6 seam, are discretized into coarse rectangular blocks with various dimensions. The bedding planes between the layers are simulated by horizontal persistent joints. Besides, to deliver more realistic modeling results, we use the CRACK and JSET command offered by UDEC to incise the polygons and blocks. In this way, we incorporate the preexisting discontinuities including bedding planes and cross joints into the pillars. The preexisting discontinuities are also assigned with suitable parameters.

3.2. Parameters Selection. In UDEC, calibration plays a critical role, owing to inconsistency in parameters such as Young's modulus (E) and uniaxial compressive strength (UCS). To achieve this calibration, the uniaxial compressive experiment was carried out to derive the complete stress-strain curve of the specimens, using a CMT5303 apparatus (Shenzhen San Si Co., China). Then, a similarly sized sample was built in UDEC with a loading rate of 0.1 m/s to calibrate the simulation parameters. With the obtained Young's modulus, the bulk modulus K and shear modulus G for the blocks in the numerical model can be calculated through the following equations [33, 34, 37]:

$$K = \frac{E}{3(1-2\mu)}, \qquad G = \frac{E}{2(1+\mu)}, \tag{1}$$

where E and μ are Young's modulus and Poisson's ratio, respectively.

The normal stiffness and shear stiffness for the contacts in the numerical model can be derived from the following equations [33, 34, 37]:

$$k_n = 10\left[\frac{K + (4/3)G}{\Delta Z_{\min}}\right], \qquad k_s = 0.4k_n, \tag{2}$$

where $\Delta Z_{\min}$ is the smallest width of the zone adjoining the contact in the normal direction.

Previous scholars used polygonal blocks in UDEC to perform sensitivity analysis on the cohesion, internal friction angle, and tensile strength of the joints [34, 42, 43]. They concluded that (1) the model tensile strength is only affected by the joint tensile strength, (2) the model internal friction angle is only affected by the joint internal friction angle, and (3) the model cohesion is affected by both the joint cohesion and internal friction angle, with the former playing a dominant role. The values of the joint cohesion, internal friction angle, and tensile strength used in this study were based on the laboratory-tested specimens and adjusted according to references [34, 35]. The simulation parameters for the rock mass are summarized in Table 1. The vertical stress exerted on the top of the model was calculated from the total weight of the overlying strata. The basal boundary is fixed in the vertical direction, and the lateral boundaries are fixed in the horizontal direction (Figure 6). Governed by the Mohr–Coulomb criterion, the model runs to an initial equilibrium loaded by gravity.

3.3. Excavation Sequence. In the model, three rooms are to be excavated firstly in the #4 seam, leaving two coal pillars in place. The three rooms are excavated simultaneously due to the following two reasons: (1) the #4 seam was mined out about two years ago and (2) this study focuses on the effect of longwall mining of the underlying seam on the stability of the residual coal pillars. Then, the #6 seam is to be excavated. The open-off cut of the longwall panel in the #6 seam is located right below the left edge of the Room I. The advance of the panel, from the left side to the right side of the model, is simulated using a stepwise excavation. Each stage involves a 10 m advance of the panel. For each stage, 10^5 time steps have been run to relieve stress and to allow the roof to cave. The total advance of the longwall panel is 120 m. To obtain a thorough understanding of the progressive failure of the coal pillars, we set up monitoring regions in the two pillars. A FISH function was custom developed to monitor and number the tensile and shear cracks generated within the pillars. To gain a thorough understanding of the progressive failure of the roof strata, we embed the measurement line in the immediate roof of the #6 seam to record the vertical stress.

4. Failure Mechanism of Residual Coal Pillar Subject to the Influence of Longwall Mining of Underlying Seam

4.1. Effect of Panel Advance on Crack Evolution in Residual Coal Pillars. Gao et al. employed UDEC to investigate crack

Table 1: Simulation parameters for the rock mass and contact.

Stratum	Matrix properties		Contact properties				
	Density ($kg \cdot m^{-3}$)	Elastic modulus (GPa)	Normal stiffness (GPa/m)	Shear stiffness (GPa/m)	Cohesion (MPa)	Internal friction angle (°)	Tensile strength (MPa)
Coarse sandstone	2480	5.6	24	5.6	3.0	33	2.3
Fine sandstone	2500	11.8	20	8.0	4.5	38	3.6
Sandy mudstone	2550	13.0	18	7.2	4.0	35	3.0
Mudstone	2450	7.3	16.0	6.4	1.8	28.0	1.5
Seam	1400	2.8	12	4.8	1.8	28.0	1.5
Contact properties for preexisting discontinuities							
Coarse sandstone			26.9	9.4	4.5	22.3	2.4
Fine sandstone			56.6	19.8	5.1	20.4	2.6
Sandy mudstone			62.4	21.8	4.9	21.2	2.4
Mudstone			7.1	2.9	1.4	18.0	0.9
Seam			8.0	3.2	0	20.0	0

generation and propagation in rocks surrounding a roadway [35]. They defined debonding between contacts along the normal direction as the tensile failure and debonding between contacts along the shear direction as the shear failure. Then the threshold was determined for tensile failure and shear failure, respectively. To capture the progressive failure of the residual coal pillars, we developed a FISH program to differentiate and count different kinds of failures. We set up monitoring regions in Pillar A and Pillar B to compute the changes of the tensile and shear cracks. Statistics for the number of the tensile and shear cracks versus model time steps are plotted in Figure 7.

As shown in Figure 7, following the excavation of the three rooms in the #4 seam, tensile and shear cracks in Pillar A and Pillar B firstly mushroom and then keep steady. It can be seen from Figure 7 that tensile cracks significantly outnumber the shear cracks, with the former about two times the number of the latter. As the panel in the #6 seam advances from A to B, increases of the tensile and shear cracks are not perceptible, meaning that Pillar A is mildly affected. At this point, the coalface is right below the left edge of Pillar A. As the panel progresses from B to C underneath Pillar A, cracks in both pillars start to grow. Unlike Pillar B, Pillar A is heavily affected over this course as evidenced by the significant increase in the number of tensile cracks. As the panel advances from C to D, cracks in both pillars grow much faster, especially in Pillar A. The fast growth of the cracks in Pillar A is attributable to dual influences of mining and roof caving. At this point, the panel advances past Pillar A by 5 m. Then the panel continues to progress and advances from D to E. Over this course, tensile cracks keep the momentum to proliferate, while the shear cracks remain dormant, exhibiting slight growth. Different from Pillar A, Pillar B is less affected as evidenced by the insignificant increase of the tensile and shear cracks. Then the panel progresses from E to F. As the panel advances under Pillar B, an interesting phenomenon appears in Figure 7. The number of tensile cracks in Pillar A fluctuates. This is caused by the closing of cracks. As for Pillar B, cracks start to grow, with the tensile cracks in particular. Then the panel continues to advance. Over the course of panel advance from F to G, in Pillar A, tensile cracks still fluctuate in number, while shear cracks gain rapid growth. Pillar B over this course is severely affected as evidenced by the rapid growth of the tensile and shear crack. As the panel advances from G to H, tensile and shear cracks in Pillar A stabilize and remain steady. The reason is that mining-induced influence on Pillar A weakens. However, tensile and shear cracks in Pillar B keep growing, indicating that Pillar B is still subject to the intense mining-induced influence.

4.2. Visualization of Crack Evolution in the Residual Coal Pillar. To visualize the development of the cracks, we handpicked some screenshots of Pillar B at various time steps, as shown in Figure 8.

To better reveal the failure mechanism of the residual pillars under the influence of longwall mining of the underlying seam, we use the FISH function offered by UDEC to visualize the evolution of tensile and shear cracks in the pillar. As mentioned above, we defined debonding between contacts along the normal direction as the tensile failure and debonding between contacts along the shear direction as the shear failure. Then the threshold was determined for tensile failure and shear failure, respectively. Another FISH program was developed to identify the polygons where tensile failure or shear failure occurred and group the polygons according to different kinds of failures. Then the two groups were highlighted in different colors. With this custom-developed FISH program, we visualize the tensile and shear cracks in the pillar. Figure 9 presents a more graphic illustration that sheds more light on crack evolution in Pillar B.

As shown in Figure 9(a), following the extraction of the three rooms in the #4 seam, cracks develop in the two ribs of the residual pillar. The cracks extend inward in a V-shape pattern in the left rib and in an arc-shape pattern in the right rib. These two failure patterns are consistent with the site observation. As the panel in the #6 seam advances, cracks in the pillar gradually propagate inward. The failure depth in the rib that is close to the advancing panel (left rib) is larger than that in the other rib. Different from the right rib, tensile failure in the left rib is the dominant failure mechanism, as shown in Figures 9(b) and 9(c). As the panel

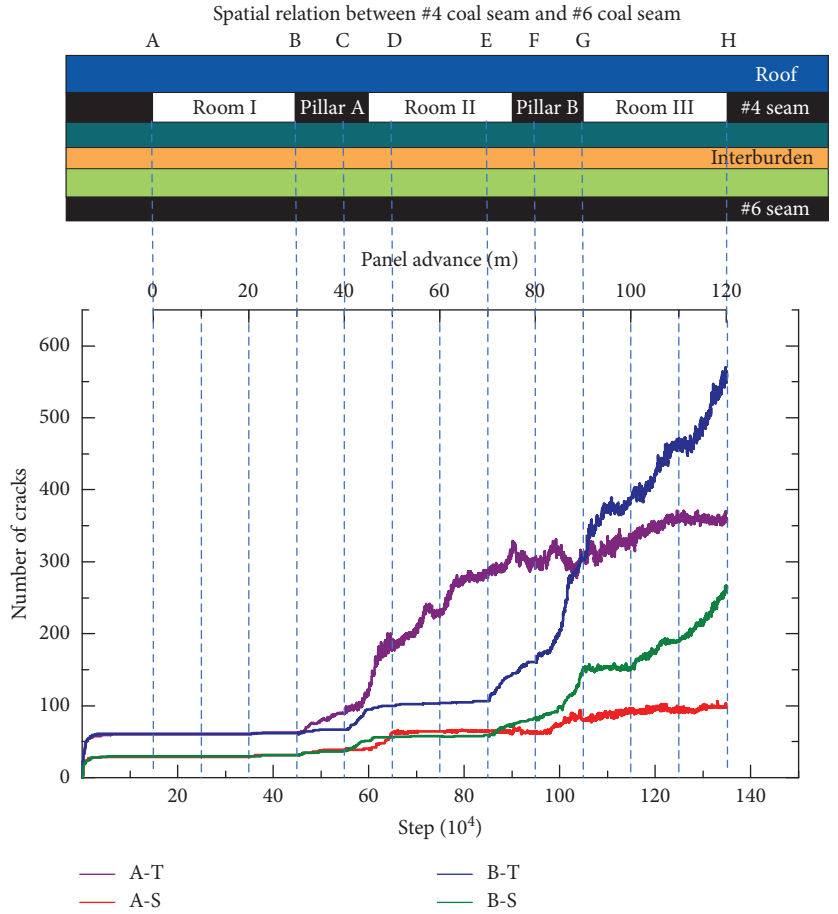

Figure 7: Number of tensile and shear cracks versus model time steps.

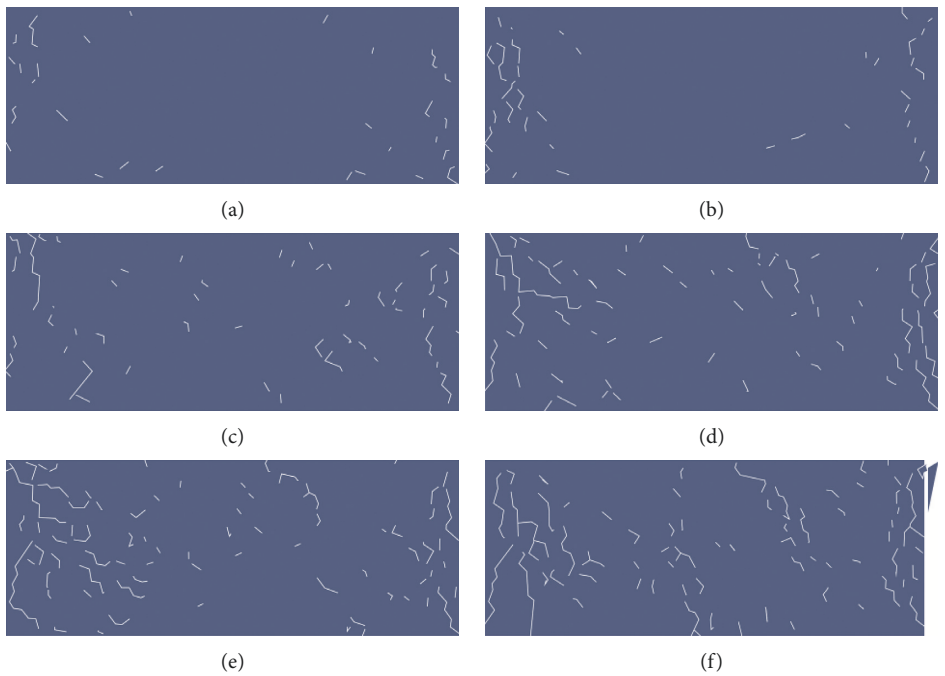

Figure 8: Crack evolution in Pillar B versus model time steps. (a) After excavation of three rooms in #4 seam. Panel in #6 seam advancing by (b) 50 m, (c) 80 m, (d) 90 m, (e) 100 m, and (f) 120 m.

Figure 9: Evolution of tensile and shear cracks in pillar B. (a) After excavation of three rooms in #4 seam. Panel in #6 seam advancing by (b) 50 m, (c) 80 m, (d) 90 m, (e) 100 m, and (f) 120 m.

continues to progress, the cracks in the center of the pillar gradually coalesce with the cracks in the two ribs, as shown in Figures 9(d) and 9(e). As the panel advances further, shear failure gains the dominant presence in the two ribs of the pillar, as shown in Figure 9(f). In the central part of the pillar, tensile failure is the dominant failure mechanism. It can also be seen from Figure 9(f) that shear failure band is intermittently distributed in the residual pillar.

4.3. Evolution of Vertical Stress in the Residual Pillar. To understand the evolution of vertical stress in Pillar B after the extraction of the #4 seam, we selected some stress contour graphs at various time steps, as shown in Figure 10. Figure 10(a) is the distribution of vertical stress after the extraction of the #4 seam. It can be seen that, after the removal of the #4 seam, the two ribs of Pillar B are in the plastic state. The plastic zone is about 0.7–0.8 m deep. Vertical stress in the two ribs decreases and is lower than the primitive stress (3.25 MPa). The central part of the pillar is in the elastic state, where the stress ranges from 8.5–10.0 MPa. Between the plastic zone and elastic zone lies the unloading zone, where the stress is highly concentrated, above 12.0 MPa. In some areas in the unloading zone, the vertical stress is up to 12.8 MPa. Therefore, the maximum stress concentration coefficient is 3.94. Overall, the vertical stress in the pillar is distributed in a saddle-shaped pattern.

As the panel in the #6 seam progresses, the unloading zone in the two sides of the pillar gradually propagates towards the center and interconnects with each other at the center of the pillar, as shown in Figures 10(b) and 10(c). It is the same with the stress concentration zones in the two ribs of the pillar. As the panel advances, the stress concentration zones gradually transfer to the center. As a result, the original elastic zone disappears. Instead, a single high-stress zone forms up, as shown in Figure 10(c).

As the advancing panel reaches the underneath of Pillar B, subject to more violent mining-induced influence, the left side of the pillar suffers more severe damage, as shown in Figure 10(c). The unloading zone transfers inward, and the high-stress zone narrows. The peak stress at the right side of the high-stress zone is 21.1 MPa (stress concentration coefficient: 6.49). As the panel continues to progress, the left side of the pillar fails completely and the high-stress zone in the pillar gradually vanishes. Stress only concentrates on the right side of the pillar, which is 12.3 MPa (stress concentration coefficient: 3.78). As shown in Figure 10(e), at this point, the unloading zone has covered most area of the pillar. Later, as the panel continues to advance, the pillar fails entirely, as shown in Figure 10(f).

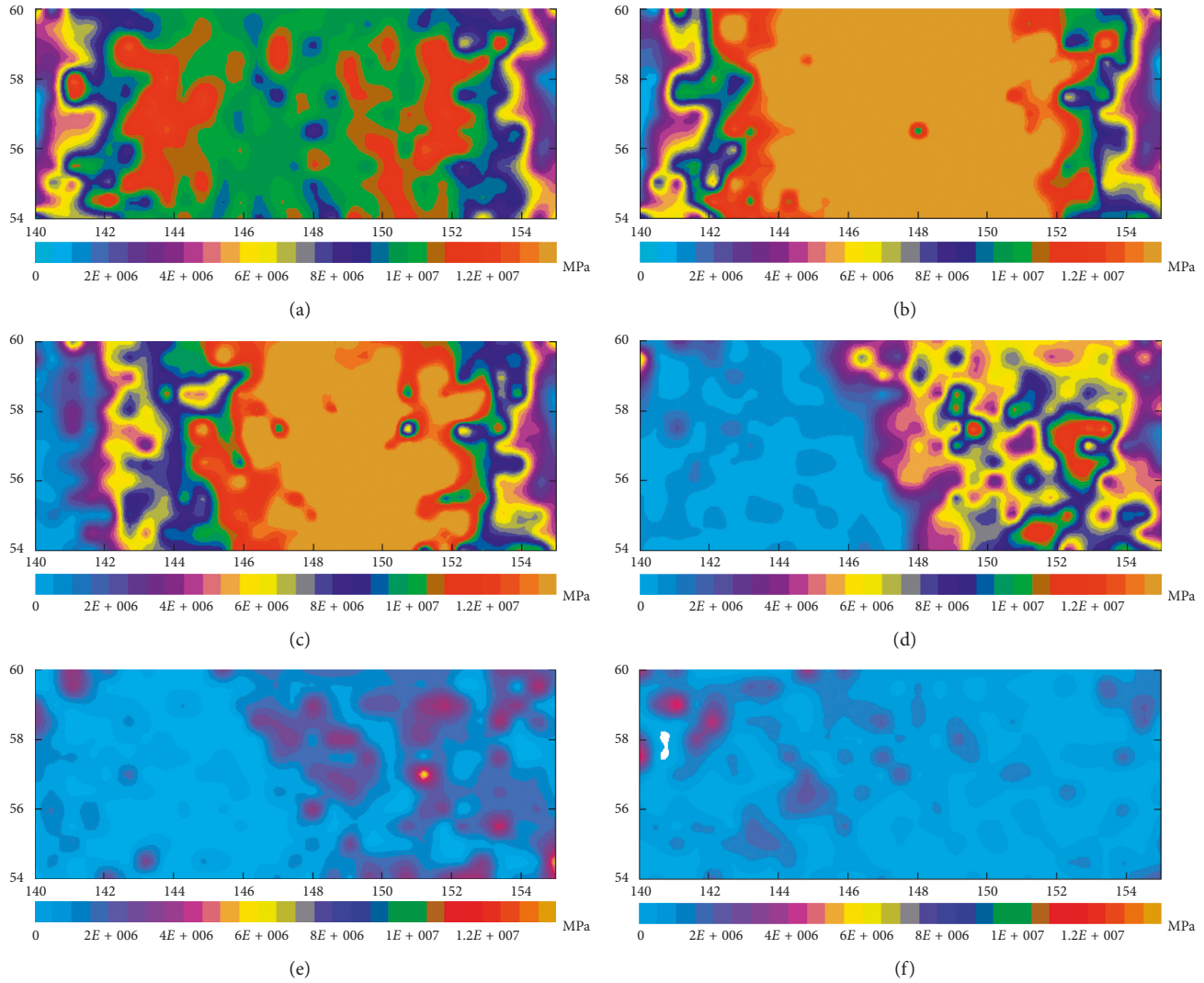

Figure 10: Evolution of vertical stress in Pillar B. (a) After excavation of three rooms in #4 seam. Panel in #6 seam advancing by (b) 50 m, (c) 80 m, (d) 90 m, (e) 100 m, and (f) 120 m.

4.4. Pillar Failure Process Analysis. We performed integrated analysis on Pillar B to gain a comprehensive understanding of pillar failure process. Figure 11 presents a set of graphs that shed more light on the failure process of the residual pillar. From top to bottom, Figure 11 presents vertical stress distribution in Pillar B, plastic zone distribution in Pillar B, shear and tensile failures distribution in Pillar B, and vertical stress distribution along the horizontal center line of Pillar B. According to Figure 11, we divide the vertical stress distribution along the horizontal center line of Pillar B into four stages: (1) "saddle shape" stage; (2) "ladder shape" stage; (3) "oblique triangle" stage; and (4) "waveform" stage.

4.4.1. First Stage: Saddle Shape. After the extraction of the #4 seam and before the removal of the #6 seam, vertical stress in Pillar B is distributed in a saddle-shaped pattern as shown in Figure 11(a4), which is a typical stress distribution pattern in the wide coal pillar. In this stage, the pillar contains two load-bearing zones, where the vertical stress exceeds the primitive stress in value. The maximum vertical stress in this stage is 12.1 MPa as shown in Figure 11(a1), and the maximum stress concentration coefficient stands at 3.72. In the middle of the pillar lies the elastic zone, where the vertical stress is larger than the primitive stress in value but less than the vertical stress in the load-bearing zone. In this zone, the vertical stress ranges from 9.5–11.5 MPa, and the stress concentration coefficient varies from 2.91–3.55. As shown in Figure 11(a2), in this zone, the coal pillar is in intact state, free from any forms of failure. In the two sides of the pillar are the fracture zones, where the polygon blocks are in the plastic state as shown in Figure 11(a2). In these zones, the strength of the coal mass weakens, and the vertical stress is less than the primitive stress as shown in Figure 11(a4).

4.4.2. Second Stage: Ladder Shape. In this stage, the panel in the #6 seam advances by 50 m and reaches the point that is 25 m away from the left edge of Pillar B. Under the mining-

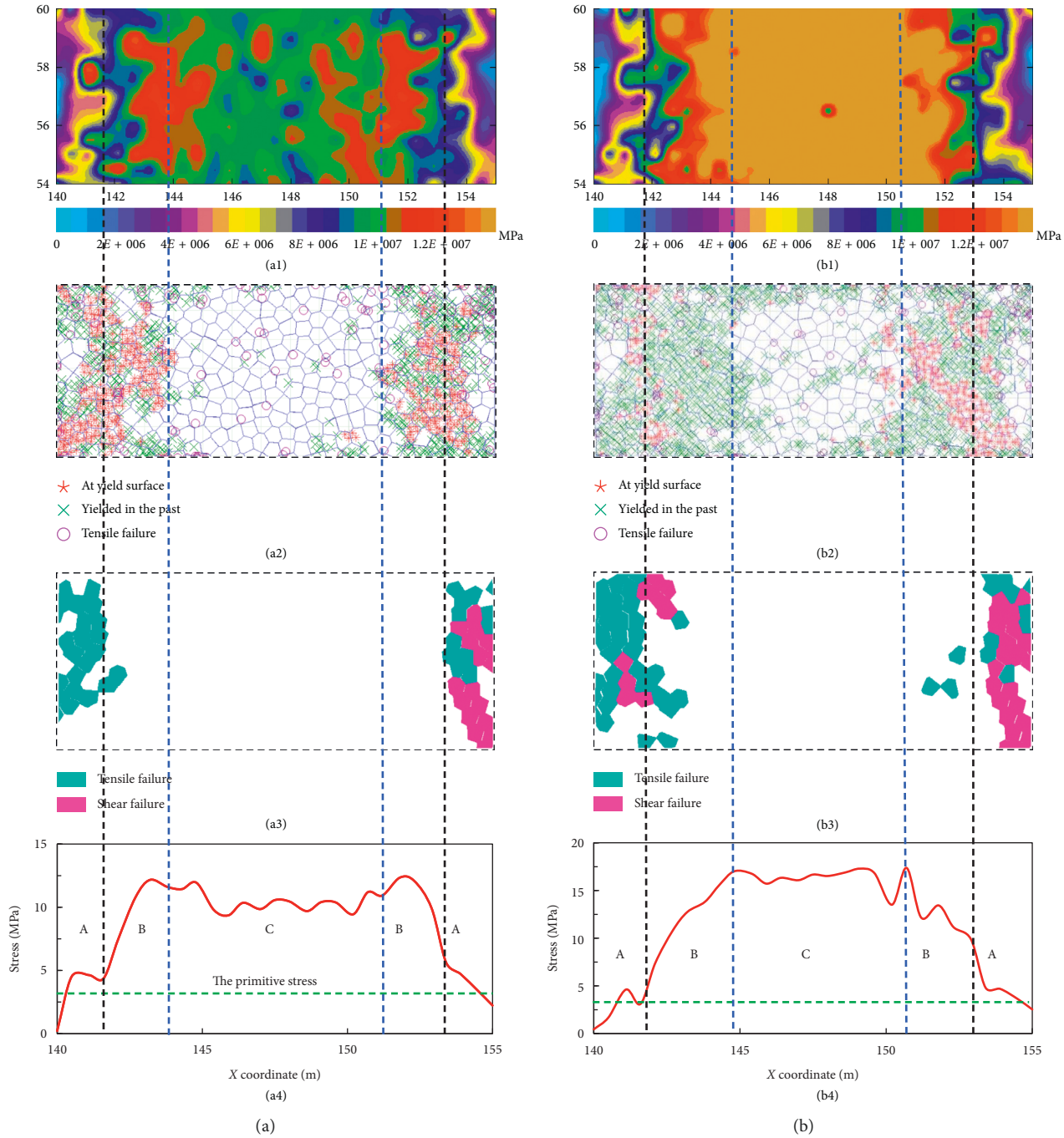

Figure 11: Continued.

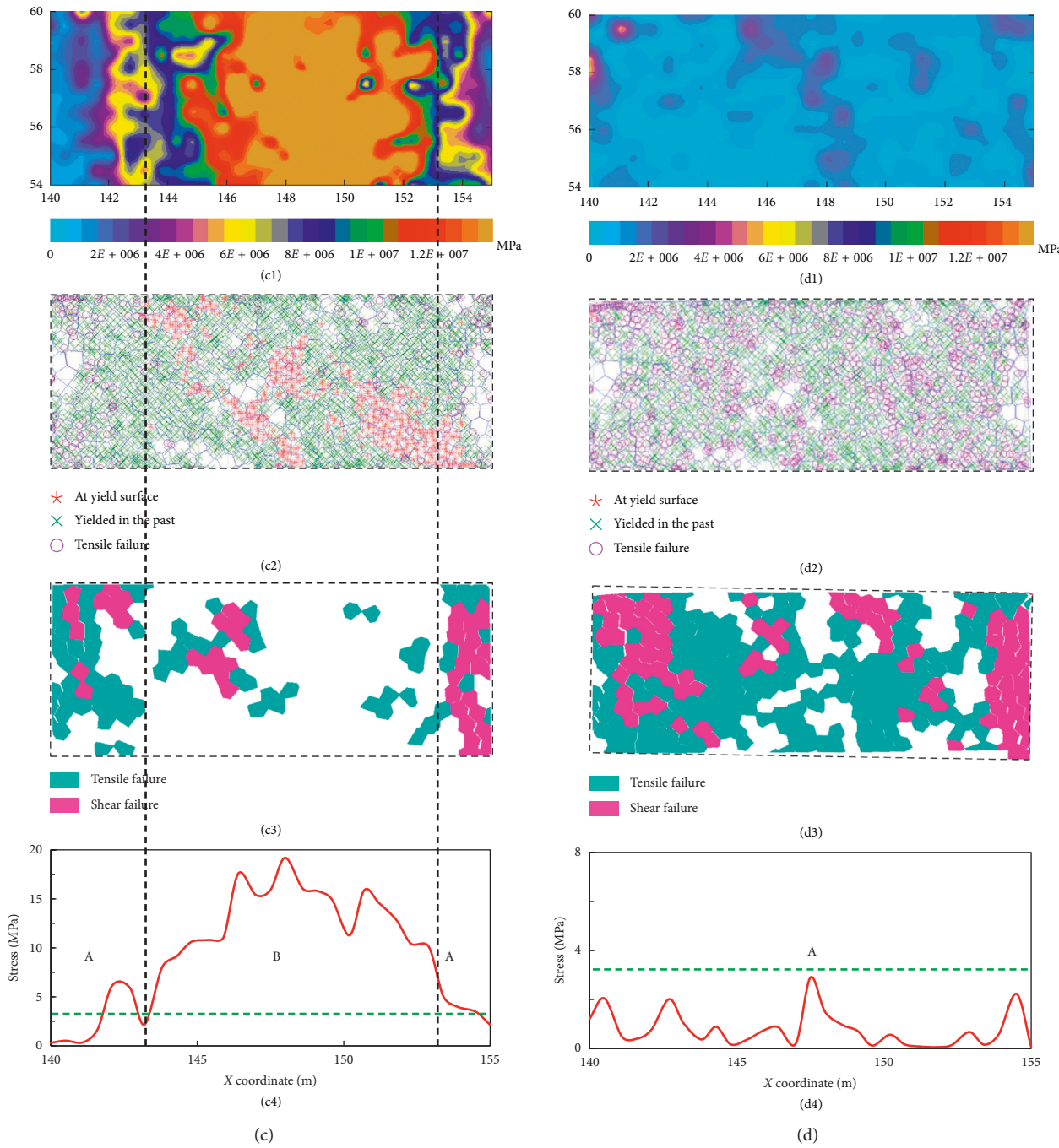

FIGURE 11: Integrated graph showing pillar failure process. (a) After excavation of three rooms in #4 seam. Panel in #6 seam advancing by (b) 50 m, (c) 80 m, and (d) 110 m. A: fracture zone (plastic zone); B: load-bearing zone (transition zone); C: elastic zone (intact zone).

induced influence, the vertical stress in Pillar B increases significantly and distributes in a ladder-shaped pattern as shown in Figure 11(b4). In this stage, the peak vertical stress at two sides of the pillar moves inward and overlaps, resulting in an extensive stress concentration zone where the stress ranges from the primitive level to the maximum level 17.4 MPa. In this stage, the vertical stress in the elastic zone rises to a high level, with an average value of 15.1 MPa (stress concentration coefficient: 4.64). Different from the "saddle shape" stage, the fracture zones at two sides of the pillar moves inward, and the elastic zone narrows.

4.4.3. Third Stage: Oblique Triangle. In this stage, the panel in the #6 seam advances by 80 m and advances past the left edge of Pillar B by 5 m. The left side of the pillar suffers severe damages, where the fracture zone expands, and the plastic zone transfers inward. In this stage, the elastic zone disappears, and virtually all the polygon blocks are in the plastic state as shown in Figure 11(c2). In addition, the plastic zone that possesses excellent bearing capacity narrows. The vertical stress along the horizontal center line of the pillar distributes in a quasi-triangular pattern as shown in Figure 11(c4). The vertical stress at the left side of the pillar is

less than that at the right side of the pillar. In the load-bearing zone, the maximum vertical stress reaches 19.2 MPa (stress concentration coefficient: 5.9). In this stage, the pillar has reached its maximum bearing capacity.

4.4.4. Fourth Stage: Waveform. In this stage, the panel in the #6 seam advances by 110 m and advances past Pillar B by 20 m. Under the combined influence of mining and roof caving, the pillar fails ultimately, with the fracture zone covering nearly the whole pillar as shown in Figure 11(d3). In this stage, the pillar loses the bearing capacity completely. The vertical stress along the horizontal center line of the pillar distributes in a wavy pattern as shown in Figure 11(d4). The residual stress decreases to a level that is less than the primitive stress.

In conclusion, longwall mining of the #6 seam results in stress redistribution. As the panel advances, the elastic zone in the pillar gradually narrows and the plastic zone in the pillar acts as a carrier that transfers stress from roof strata to floor strata. As the fracture zones at two sides of the pillar move inward, the effective load-bearing zone narrows, leading to significant stress increase. In this stage, the stress in the pillar can exert an adverse impact on the safe extraction of the underlying adjoining seam under the residual pillars. Ultimately, as the panel advances past the pillar, the pillars along with the roof strata above the #6 seam fail. The pillars are only left with the residual bearing capacity.

5. Overlying Strata Movement of a Longwall Mining Face in an Abutting Seam beneath a Room Mining Gob

The distance between the seams is a crucial factor that affects the safe removal of the seam underlying the mined-out area or gob. For example, if the underlying seam is adjacent to the overlying mined-out area, it is highly possible that the caving zone resulting from longwall mining of the underlying seam could interconnect with the overlying mined-out area. The interconnection could lead to the rapid ingress of the gob water and gas into the coalface in production, posing a significant threat to mining safety. Also, the stability of the irregular coal pillar left in the mined-out area can have a substantial effect on the behavior of the mining pressure in the underlying panel. Therefore, it is of great engineering significance to investigate the characteristics of overlying strata movement in the longwall mining of an adjoining seam underlying a gob left by room mining.

5.1. Progressive Failure of Overlying Strata. Figure 12 presents the progressive failure of the strata overlying the #6 seam as the panel advances. In the initial stage, room-and-pillar mining is modeled in the 3 m thick #4 seam, which results in the exposing of the immediate roof. As shown in Figure 12(a), in this stage, the roof strata maintain good integrity and only a small fraction of cracks appear. This modeling result is consistent with the site survey.

After the panel advances by 40 m, roof strata above the #4 seam still maintain good integrity, with no occurrence of caving. Though the larger area of roof strata above the #6 seam is exposed after panel advance, the roof strata are in good condition. Only a small portion of rocks caves to the gob, as shown in Figure 12(b). This is due to the reason that the immediate roof of the #6 seam is made of 7.5 m thick coarse sandstone, which possesses a higher compressive strength. Therefore, it can maintain its integrity and stability over a larger span.

As shown in Figure 12(c), with the further advance of the panel, a massive amount of traverse cracks appears in the immediate roof of the #6 seam and the beam-like roof bends and fractures. As a result, a significant portion of rocks caves to the gob. 28 m high above the #4 seam lays an 8 m thick siltstone, which is the key stratum [44–46]. In this stage, bed separation occurs between this rock layer and the 3–1 seam below.

After the panel advances by 80 m, the immediate roof of the #6 seam fractures entirely and cracks begin to develop in the overlying 3.5 m thick fine sandstone and 5 m thick sandy mudstone due to deformation. At this stage, the immediate roof of the #4 seam fractures and cracks start to develop in the main roof and proliferate all the way up to the rock layer beneath the key stratum. As the roof strata above the #6 seam sag or subside, separation below the key stratum exacerbates (Figure 12(d)).

As shown in Figure 12(e), after the panel progresses by 100 m, a great number of cracks appear in the fine sandstone and sandy mudstone above the #6 seam and the overlying strata deform and subside further. Figure 12(f) illustrates the state of the overlying strata after the panel advances by 120 m. It can be seen that the roof strata above the #6 seam cave entirely and the roof strata above the #4 seam subside as a result of the caving. It can also be seen that the separation below the key stratum extends over a larger area.

5.2. Evolution of Vertical Stress in #6 Seam Roof. In the mining of seams in proximity, residual coal pillars act as carriers that transfer stress from the overlying strata to the underlying strata, resulting in stress redistribution in the underlying seam. Therefore, the residual pillar-induced stress concentration exerts a profound influence on safe mining under pillars. To probe into the evolution of vertical stress in the roof of the #6 seam during panel extraction, we set up 16 measurement points in the immediate roof of the #6 seam to record the stress. As shown in Figure 13, at an interval of 10 m, the measurement points are distributed over a straight line that is 0.8 m away from the #6 seam.

According to the location of the stress measurement points, we plot the stress versus model time steps in three graphs as presented in Figure 14.

Figure 14(a) presents the evolution of the vertical stress recorded by the measurement points under solid coal seams (P1, P2, P15, and P16). Measurement points P1 and P2 record the rear abutment stress. The stress shows the following characteristics: (1) as the panel advances, the stress gradually increases; (2) when the panel is advancing beneath the coal pillar, the stress rises significantly; and (3) during the first roof weighting, the stress also rises rapidly. After the

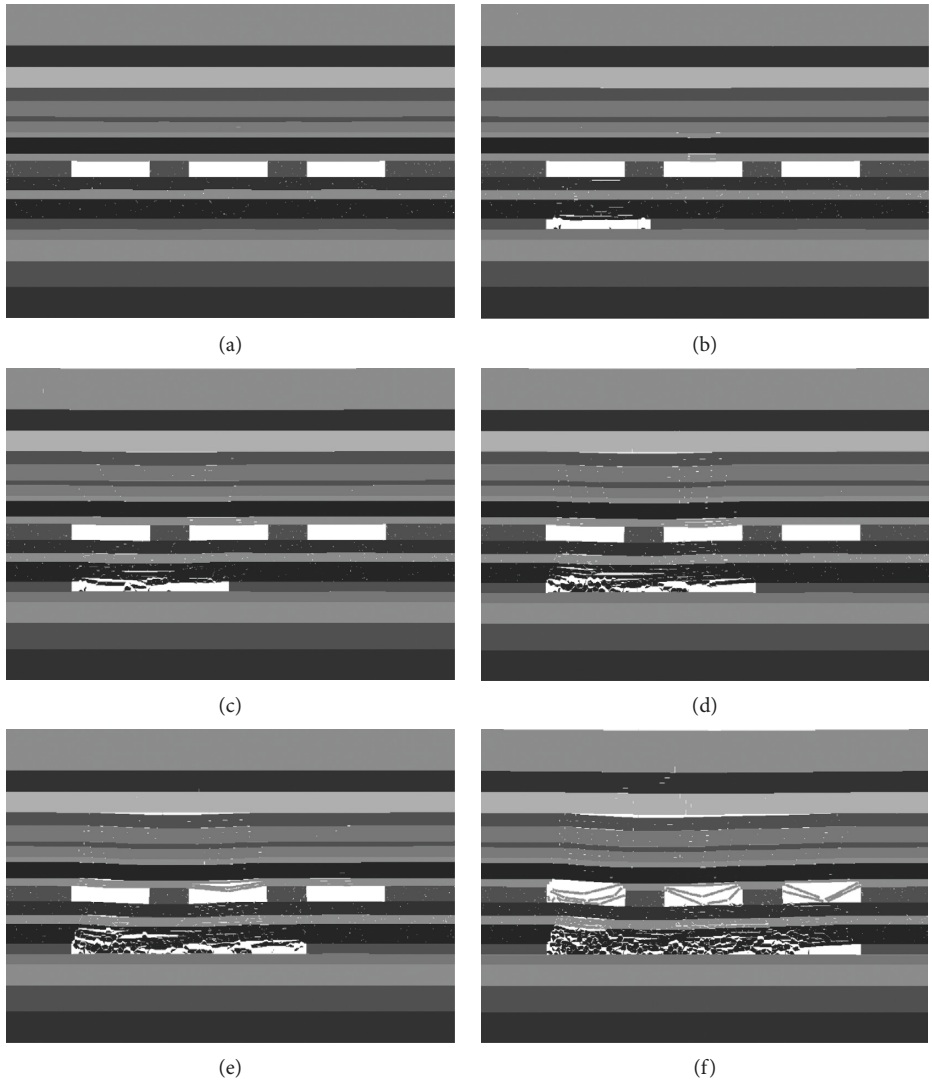

Figure 12: Progressive caving of overlying strata during the advance of panel in the #6 seam. (a) 0 m. (b) 40 m. (c) 60 m. (d) 80 m. (e) 100 m. (f) 120 m.

panel progresses by over 100 m, the stress levels off, indicating that the stress has reached a new equilibrium. As for measurement points P15 and P16, they record the front abutment stress. The recorded stress shows distinctive characteristics: (1) when the panel reaches the point that is right below Pillar A, the stress slowly rises and soon stabilizes; (2) after the panel advances past Pillar B, the stress rises significantly; and (3) when the advancing panel is 20 m away from measurement point P15, the stress rises rapidly, indicating that the area now is within the scope of influence of the front abutment stress.

Figure 14(b) presents the evolution of the vertical stress recorded by the measurement points located in the floor of #4 seam with concentrated stress caused by the residual pillars (P5, P6, P7, P10, P11, and P12) and the boundary of the mining area (P14). The stresses recorded by these measurement points can be divided into three stages based on their characteristics. In the first stage, the stresses rise due to the extraction of the #4 seam; in the second stage, the stresses increase as the advancing panel in the #6 seam is approaching; in the third stage, the stresses fall to a very low level due to the complete failure of the residual coal pillars. Just take the measurement point P11 as an example. After the extraction of the #4 seam, this point locates within the stress concentration zone caused by the presence of the residual coal pillar. The vertical stress is about 6 MPa; when the panel in the #6 seam advances by 30 m, the recorded stress starts to rise; when the panel advances by 40 m, the recorded stress rises significantly; when the panel advances by 70 m, the recorded stress rises rapidly and reaches the maximum level of 13.2 MPa (stress concentration coefficient: 4.1); as the panel advances further, the recorded stress plummets to about zero. The stress recorded by measurement point P7 shares similar characteristics with measurement point P11. Therefore, according to the recorded stress, we conclude that the scope of influence of the front abutment stress during longwall mining beneath the residual pillars is 40–50 m, and the front abutment stress reaches its peak about 10 m ahead of the advancing panel.

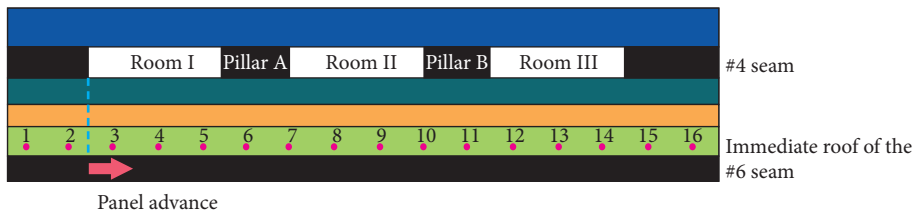

Figure 13: Stress measurement points embedded in the immediate roof of the #6 seam.

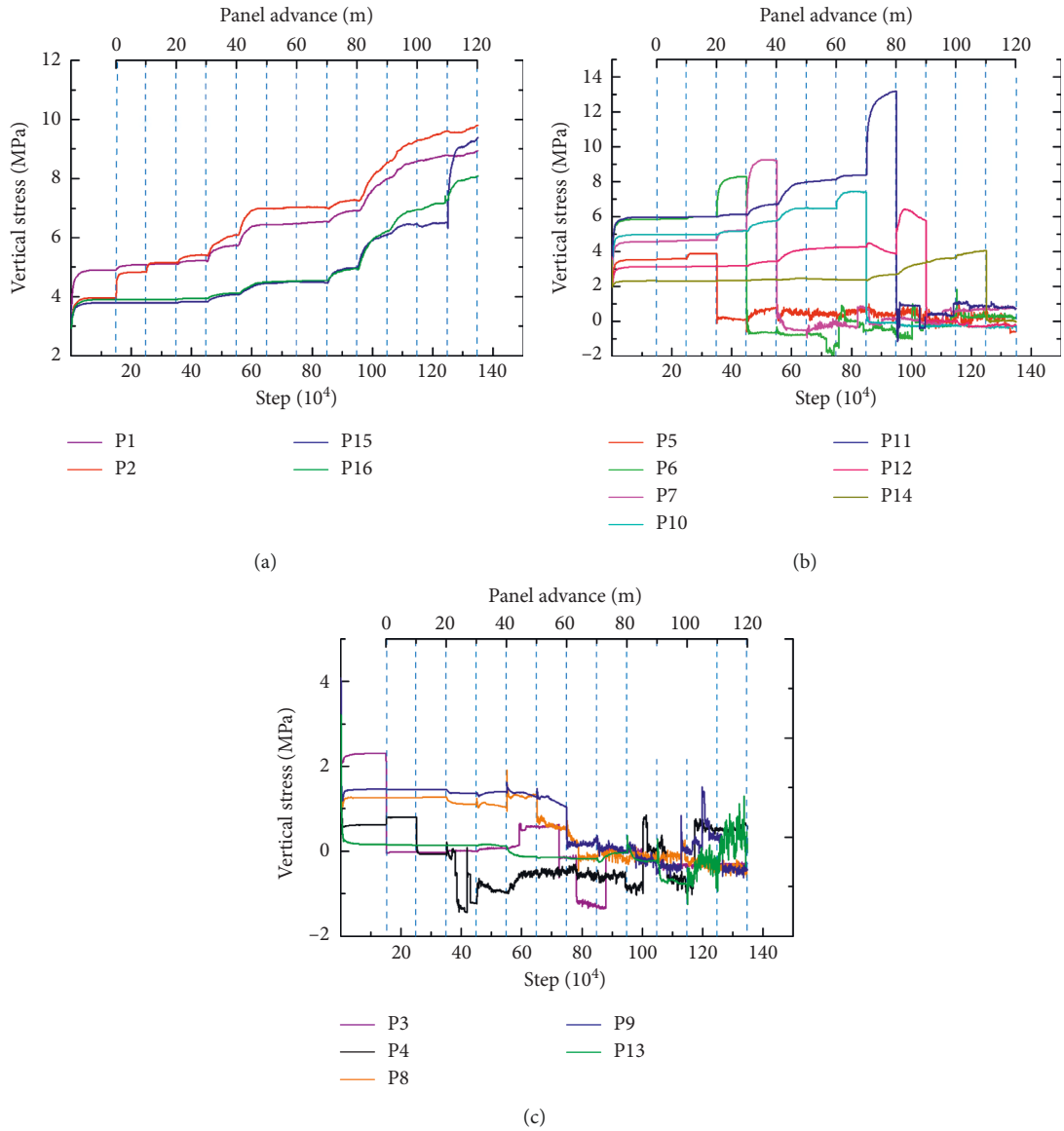

Figure 14: Evolution of vertical stress in the immediate roof of the #6 seam. (a) Under solid coal seam. (b) Under residual coal pillars. (c) Under mined-out area.

Figure 14(c) presents the evolution of the vertical stress recorded by the measurement points under mined-out area (P3, P4, P8, P9, and P13). These measurement points record the stress within the stress relief zone. After the extraction of the #4 seam, the stresses are low, ranging from 0.2 MPa to 2.2 MPa. When the advancing panel has not reached the measurement point, the stress is slightly influenced by the front abutment stress, and the maximum stress is only about 1.9 MPa. After the panel has advanced past the measurement point, the stress reduces to about zero and undergoes slight fluctuation.

6. Measures to Guarantee Safe Longwall Mining beneath Room Mining Gob

From the above study, we obtain the following findings: (1) the scope of influence of the front abutment stress during longwall mining beneath the residual pillars is 40–50 m; (2) the front abutment stress reaches its peak about 10 m ahead of the advancing panel; and (3) under the residual pillar, the maximum front abutment stress could reach 13.2 MPa (stress concentration coefficient: 4.1). Therefore, as the panel approaches and advances beneath the pillars left in the #4 seam, it is very likely that the mining pressure behaves violently. As a result, a host of problems can occur, such as hydraulic support jamming, coal pillar spalling, serve roadway deformation, and uncontrolled roof caving, posing a significant threat to mining safety. With reference of previous research achievement, we propose the following workable measures to guarantee safe longwall mining in panel 6104 and panel 6105 in Yuanbaowan mine (Figure 15).

(1) Handle the mined-out area in the #4 seam. As the #4 seam was extracted using unconventional mining method, the mined-out area and the residual pillars are unmatched in dimension. Therefore, the residual pillars cannot sustain long-term stability and the presence of these pillars can cause catastrophic stress concentration. Two measures can be taken to address this problem. The first one is to force the roof strata to cave artificially. In places where a large area of roof strata are exposing, the loosening blasting method can be employed to fracture the roof and residual pillars, forcing the roof strata to cave. The second one is to backfill the mined-out area with sand or quick-setting cement.

(2) Optimize longwall mining in the #6 seam. Measures such as selecting a suitable mining height, quickening panel advance, strengthening support management, and using proper hydraulic support can bring the mining pressure under control.

The site survey shows that mined-area in the #4 seam is in a complicated situation. Besides, loosening blasting and backfilling are not only difficult to implement but also cost ineffective. Therefore, optimizing the longwall mining in the #6 seam is a preferred choice.

7. Conclusions

Sustainable development of coal industry is critically significant for the national economy and social development. Hence, it is very important to increase the coal recovery rate, to extract coal seams with complex conditions, and to reduce mine accidents. Recent years have witnessed the increase of longwall mining in adjoining seams beneath room mining gob. Longwall mining of the abutting seam with the presence of the residual coal pillars overlying the seam can result in abnormal strata pressure and severe overburden failure, which poses a significant threat to mining safety. The threat mainly manifests itself in the form of intense roof weighting and hazardous interconnection between the gobs. Therefore, it has become a significant challenge to achieve safe mining under residual pillars. To address this challenge, we took the #6 coal seam in the Yuanbaowan Mine, China, as an example and numerically investigated the failure mechanism of the residual coal pillars under the influence of longwall mining in a seam beneath room mining gob and revealed the dynamic evolution of stress and crack in residual coal pillars. We also proposed effective measures to ensure safe extraction under the residual coal pillars. The main conclusions from this study are summarized as follows:

(1) A FISH function was custom developed to monitor and number the tensile and shear cracks generated within the residual pillars. It is found that, after the extraction of the #4 seam, tensile cracks significantly outnumber the shear cracks in the pillars, with the former about two times the number of the latter. As the panel advances in the #6 seam, cracks in the pillar ribs gradually propagate inward. The rib that is more adjacent to the advancing panel suffers more severe failure, with the tensile failure playing a dominant role. As the panel continues to progress, the cracks in the center of the pillar gradually coalesce with the cracks in the two ribs. The shear failure band is intermittently distributed in the residual pillar, and tensile failure is the dominant failure mechanism in the central part of the pillar.

(2) Based on the integrated analysis, we divided the vertical stress distribution along the horizontal center line of the pillar into four stages: (1) "saddle shape" stage; (2) "ladder shape" stage; (3) "oblique triangle" stage; and (4) "waveform" stage.

(3) The characteristics of overlying strata movement in the longwall mining of an adjoining seam beneath a room mining gob were revealed. In the initial stage, after the extraction of the #4 seam, the roof strata above the #4 seam maintain good integrity and only a small fraction of cracks appear. The modeling results show good agreement with the site survey. After the panel advances by 40 m, roof strata above the #4 seam still maintain good integrity. Though a larger area of roof strata above the #6 seam is exposed after panel advance, the roof strata are in the favorable condition. Only a small portion of rocks caves to the gob. With the further progress of the panel, a massive amount of traverse cracks appears in the immediate roof of the #6 seam and the beam-like roof bends and fractures. After the panel advances by 80 m, the immediate roof of the #6 seam fractures entirely and cracks begin to develop in the overlying 3.5 m thick fine sandstone and 5 m thick sandy mudstone. At this stage, the immediate roof of the #4 seam fractures and cracks start to develop in the main roof and propagate all the way up to the rock layer beneath the key stratum. After the panel advances by 120 m, the roof strata above the #6 seam cave entirely and the

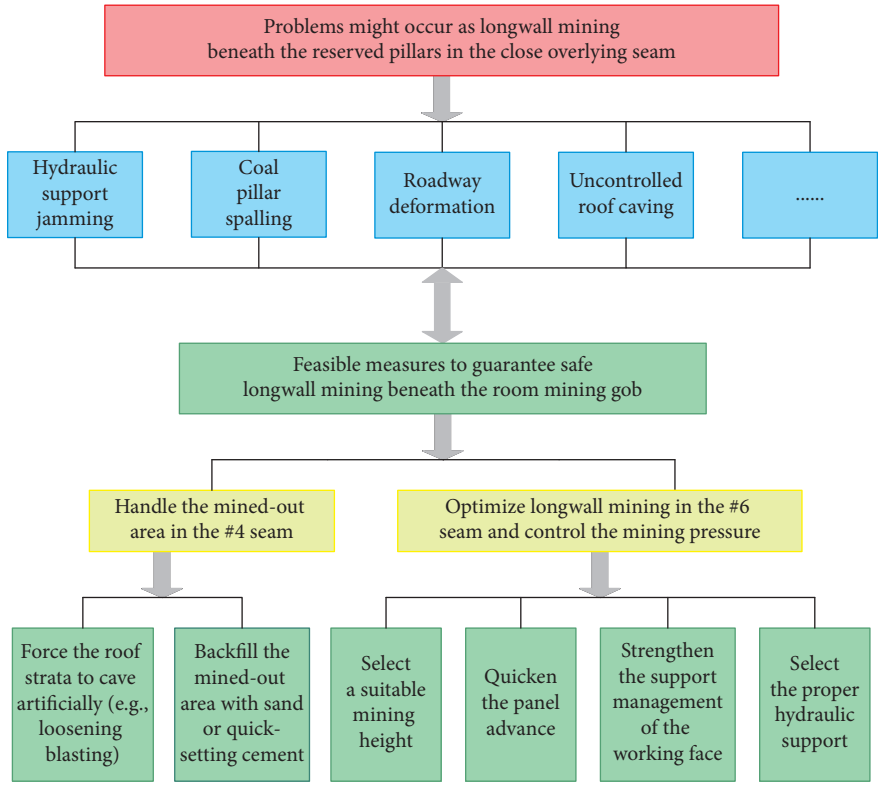

Figure 15: Block diagram of proposed measures to guarantee safe longwall mining beneath room mining gob.

roof strata above the #4 seam subside as a result of the caving. At this stage, separation below the key stratum extends over a larger area.

(4) As the panel progresses, the rear abutment stress gradually increases. When the panel is advancing beneath the coal pillar, the stress rises significantly. After the panel advances by over 100 m, the stress levels off. Under the influence of the pillars left in the #4 seam, the scope of influence of the front abutment stress during longwall mining is 40–50 m, and the front abutment stress reaches its peak about 10 m ahead of the advancing panel.

(5) The overlap of the front abutment stress induced by mining in the #6 seam with the concentrated stress in the pillar floor can reach a maximum stress level up to 13.2 MPa (stress concentration coefficient: 4.1). Therefore, as the panel approaches and advances beneath the residual pillars, it is very likely that the mining pressure behaves violently. As a result, a host of problems can occur, such as hydraulic support jamming, coal pillar spalling, serve roadway deformation, and uncontrolled roof caving, posing a significant threat to mining safety. To guarantee safe longwall mining in Yuanbaowan mine, we propose some workable measures.

Data Availability

All the data included in this study are available upon request from the corresponding author.

Conflicts of Interest

The authors declare that they have no conflicts of interest.

Acknowledgments

Financial support for this work, provided by the National Natural Science Foundation of China (No. 41602174), the Open Projects of Research Center of Coal Resources Safe Mining and Clean Utilization, Liaoning (LNTU17KF02), the Independent Research Project of State Key Laboratory of Coal Resources and Safe Mining, China University of Mining and Technology (SKLCRSM18X014), the Fundamental Research Funds for the Central Universities (2015XKZD04), and the Priority Academic Program Development of Jiangsu Higher Education Institutions (PAPD), is gratefully acknowledged.

References

[1] G. Jin, L. Wang, J. Zhang, M. Hu, and N. Duan, "Roadway layout for recycling residual coal pillar in room-and-pillar mining of thick coal seam," *International Journal of Mining Science and Technology*, vol. 25, no. 5, pp. 729–734, 2015.

[2] S. Tu, F. Wang, F. Dou, Y. Yuan, and Y. Lu, "Fully mechanized top coal caving: underground stress at gateways under barrier pillars of an upper coal seam," *Journal of China University of Mining and Technology*, vol. 39, no. 1, pp. 1–5, 2010, in Chinese.

[3] F. Wang, S. Tu, Z. Li, H. Tu, and F. Chen, "Mutation instability mechanism of the room mining residual pillars in the shallow depth seam," *Journal of Mining and Safety Engineering*, vol. 29, no. 6, pp. 770–775, 2012, in Chinese.

[4] F. Wang, C. Zhang, X. Zhang, and Q. Song, "Overlying strata movement rules and safety mining technology for the shallow depth seam proximity beneath a room mining goaf," *International Journal of Mining Science and Technology*, vol. 25, no. 1, pp. 139–143, 2015.

[5] F. Wang, C. Duan, S. Tu, N. Liang, and Q. Bai, "Hydraulic support crushed mechanism for the shallow seam mining face under the roadway pillars of room mining goaf," *International Journal of Mining Science and Technology*, vol. 27, no. 5, pp. 853–860, 2017.

[6] J. Yang, C. Liu, Y. Yang, and J. Li, "Study of the bearing mechanism of the coal roof and the dimension selection of the room and pillar in the shallow and close distance coal seam," *Journal of China University of Mining & Technology*, vol. 42, no. 2, pp. 161–168, 2013, in Chinese.

[7] D. Zhu and S. Tu, "Mechanisms of support failure induced by repeated mining under gobs created by two-seam room mining and prevention measures," *Engineering Failure Analysis*, vol. 82, pp. 161–178, 2017.

[8] D. Zhu, S. Tu, H. Tu, and Z. Yang, "Mechanisms of support failure and prevention measures under double-layer room mining gobs–a case study: shigetai coal mine," *International Journal of Mining Science and Technology*, 2018, In press.

[9] C. Mark, F. E. Chase, and D. M. Pappas, "Analysis of multiple seam stability," in *Proceedings of the 26th International Conference on Ground Control Mining*, pp. 5–18, Morgantown, WV, USA, July-August 2007.

[10] J. L. Ellenberger, F. E. Chase, and C. Mark, "Using site case histories of multiple seam coal mining to advance mine design," in *Proceedings of the 22nd International Conference on Ground Control in Mining*, pp. 59–64, Morgantown, WV, USA, August 2003.

[11] W. J. Gale, "Rock fracture, caving and interaction of face supports under different geological environments. Experience from Australian coal mine," in *Proceedings of the 23rd International Conference on Ground Control in Mining*, pp. 11–19, Morgantown, WV, USA, August 2004.

[12] R. K. Zipf, "Failure mechanics of multiple seam mining interactions," in *Proceedings of the 24th International Conference on Ground Control in Mining*, pp. 93–106, Morgantown, WV, USA, August 2005.

[13] K. Morsy, A. Yassien, and S. Peng, "Multiple seam mining interactions–a case study," in *Proceedings of the 25th International Conference on Ground Control in Mining*, pp. 308–314, Morgantown, WV, USA, August 2006.

[14] W. J. Gale, "Multi-seam layout guidelines and feasibility of partial chain pillar removal," Final Report, Australian Coal Association Research Program by Mining Research and Consulting Group, Brisbane, Australia, 2004.

[15] N. C. Zhang, N. Zhang, J. Esterle, J. G. Kan, Y. M. Zhao, and F. Xue, "Optimization of gateroad layout under a remnant chain pillar in longwall undermining based on pressure bulb theory," *International Journal of Mining Reclamation and Environment*, vol. 30, no. 2, pp. 128–144, 2015.

[16] M. Christopher and A. Zach, "Analysis of coal pillar stability (ACPS): a new generation of pillar design software," *International Journal of Mining Science and Technology*, vol. 29, no. 1, pp. 87–91, 2019.

[17] P. Zhang, S. Peterson, D. Neilans, S. Wade, R. McGrady, and J. Pugh, "Geotechnical risk management to prevent coal outburst in room-and-pillar mining," *International Journal of Mining Science and Technology*, vol. 26, no. 1, pp. 9–18, 2016.

[18] M. S. HA. Underground, "Coal mine, fatal rib roof accident. Report of investigation," 2006, http://www.msha.gov/fatals/2006/ftl06c18.asp.

[19] C. Wang, "*Research on the structure and support load analysis of fully-mechanized mining face in close distance coal seam under goaf*," M.S. thesis, Taiyuan University of Technology, Taiyuan, China, 2013.

[20] J. Ju, J. Xu, W. Zhu, and X. Wang, "Mechanism of strong strata behaviors during the working face out of the upper dip coal pillar in contiguous seams," *Journal of China Coal Society*, vol. 35, no. 1, pp. 15–20, 2010, in Chinese.

[21] J. Ju and J. Xu, "Influence of leading instability in the upper dip coal pillar boundary to the strong strata behaviors during the working face out of the pillar," *Journal of China Coal Society*, vol. 37, no. 7, pp. 1080–1087, 2012, in Chinese.

[22] J. Ju and J. Xu, "Prevention measures for support crushing while mining out the upper coal pillar in close distance shallow seams," *Journal of Mining and Safety Engineering*, vol. 30, no. 3, pp. 323–330, 2013, in Chinese.

[23] J. Ju, J. Xu, and W. Zhu, "Longwall chock sudden closure incident below coal pillar of adjacent upper mined coal seam under shallow cover in the Shendong coalfield," *International Journal of Rock Mechanics and Mining Sciences*, vol. 77, pp. 192–201, 2015.

[24] X. T. Feng, S. F. Pei, Q. Jiang, Y. Y. Zhou, S. J. Li, and Z. B. Yao, "Deep fracturing of the hard rock surrounding a large underground cavern subjected to high geostress: in situ observation and mechanism analysis," *Rock Mechanics and Rock Engineering*, vol. 50, no. 8, pp. 2155–2175, 2017.

[25] G. Reed, K. Mctyer, and R. Frith, "An assessment of coal pillar system stability criteria based on a mechanistic evaluation of the interaction between coal pillars and the overburden," *International Journal of Mining Science and Technology*, vol. 27, no. 1, pp. 9–15, 2017.

[26] W. Yang, C. Liu, B. Huang, and Y. Yang, "Determination on reasonable malposition of combined mining in close-distance coalseams," *Journal of Mining & Safety Engineering*, vol. 29, no. 1, pp. 101–105, 2012, in Chinese.

[27] T. Hauquin, O. Deck, and Y. Gunzburger, "Average vertical stress on irregular elastic pillars estimated by a function of the relative extraction ratio," *International Journal of Rock Mechanics and Mining Sciences*, vol. 83, pp. 122–134, 2016.

[28] E. F. Salmi, M. Nazem, and M. Karakus, "The effect of rock mass gradual deterioration on the mechanism of post-mining subsidence over shallow abandoned coal mines," *International Journal of Rock Mechanics and Mining Sciences*, vol. 91, pp. 59–71, 2017.

[29] E. Walls, P. Mpunzi, and W. Joughin, "Room and pillar stability analysis using linear elastic modelling and probability of failure—a case study," in *Proceedings of the International Seminar on Design Methods in Underground Mining*, Y. Potvin, Ed., pp. 95–106, Australian Centre for Geomechanics, Perth, Australia, 2015.

[30] H. Maleki, "Coal pillar mechanics of violent failure in U.S. Mines," *International Journal of Mining Science and Technology*, vol. 27, no. 3, pp. 387–392, 2017.

[31] P. Waclawik, J. Ptacek, P. Konicek, R. Kukutsch, and J. Nemcik, "Stress-state monitoring of coal pillars during room and pillar extraction," *Journal of Sustainable Mining*, vol. 15, no. 2, pp. 49–56, 2016.

[32] E. Ghasemi, H. Kalhori, and R. Bagherpour, "Stability assessment of hard rock pillars using two intelligent classification techniques: a comparative study," *Tunnelling and Underground Space Technology*, vol. 68, pp. 32–37, 2017.

[33] Itasca Consulting Group Inc., *UDEC (Universal Distinct Element Code), Version 4.1*, Itasca, Minneapolis, MN, USA, 2011.

[34] F. Q. Gao and D. Stead, "The application of a modified Voronoi logic to brittle fracture modelling at the laboratory and field scale," *International Journal of Rock Mechanics and Mining Sciences*, vol. 68, pp. 1–14, 2014.

[35] F. Gao, D. Stead, and J. Coggan, "Evaluation of coal longwall caving characteristics using an innovative UDEC Trigon approach," *Computers and Geotechnics*, vol. 55, pp. 448–460, 2014.

[36] F. Gao, D. Stead, H. Kang, and Y. Wu, "Discrete element modelling of deformation and damage of a roadway driven along an unstable goaf-a case study," *International Journal of Coal Geology*, vol. 127, no. 1, pp. 100–110, 2014.

[37] X. Li, M. Ju, Q. Yao, J. Zhou, and Z. Chong, "Numerical investigation of the effect of the location of critical rock block fracture on crack evolution in a gob-side filling wall," *Rock Mechanics and Rock Engineering*, vol. 49, no. 3, pp. 1041–1058, 2016.

[38] M. Havaej, D. Stead, E. Eberhardt, and B. R. Fisher, "Characterization of bi-planar and ploughing failure mechanisms in footwall slopes using numerical modelling," *Engineering Geology*, vol. 178, pp. 109–120, 2014.

[39] F. Gao, D. Stead, and H. Kang, "Simulation of roof shear failure in coal mine roadways using an innovative UDEC Trigon approach," *Computers and Geotechnics*, vol. 61, pp. 33–41, 2014.

[40] F. Gao and D. Stead, "Discrete element modelling of cutter roof failure in coal mine roadways," *International Journal of Coal Geology*, vol. 116-117, pp. 158–171, 2013.

[41] S. Tian, X. Cui, and Y. Gong, "An approach to generate spatial Voronoi Treemaps for points, lines, and polygons," *Journal of Electrical and Computer Engineering*, vol. 2015, Article ID 787163, 10 pages, 2015.

[42] T. Kazerani and J. Zhao, "Micromechanical parameters in bonded particle method for modelling of brittle material failure," *International Journal for Numerical and Analytical Methods in Geomechanics*, vol. 34, no. 18, pp. 1877–1895, 2010.

[43] T. Kazerani, "Effect of micromechanical parameters of microstructure on compressive and tensile failure process of rock," *International Journal of Rock Mechanics and Mining Sciences*, vol. 64, pp. 44–55, 2013.

[44] M. Qian, X. Miao, J. Xu, and X. Mao, *Study of Key Strata Theory in Ground Control*, China University of Mining and Technology Press, Xuzhou, China, 2003.

[45] J. Xu and M. Qian, "Method to distinguish key strata in overburden," *Journal of China University of Mining and Technology*, vol. 29, no. 5, pp. 463–467, 2000, in Chinese.

[46] S. Liang, D. Elsworth, X. Li, X. Fu, B. Sun, and Q. Yao, "Key strata characteristics controlling the integrity of deep wells in longwall mining areas," *International Journal of Coal Geology*, vol. 172, pp. 31–42, 2017.